Nature Environment and Pollution Technology
An International Quarterly Scientific Journal

ISSN: 0972-6268	Vol. 12	No. 1	pp. 1-6	2013

Original Research Paper

Diurnal Evolution of Solar Radiation in UV, PAR and NIR Bands in High Air Masses

Jackson H. W. Chang, Jedol Dayou and Justin Sentian*
Energy, Vibration and Sounds Research Group (e-VIBS), School of Science & Technology, UMS, Jalan UMS, 88400, Kota Kinabalu, Malaysia
*Climate Change Research Group (CCRG), School of Science & Technology, UMS, Jalan UMS, 88400, Kota Kinabalu, Malaysia

Nat. Env. & Poll. Tech.
Website: www.neptjournal.com
Received: 15-11-2012
Accepted: 3-12-2012

Key Words:
Diurnal evolution
Solar radiation
High air masses
Water vapour
Aerosol

ABSTRACT

Solar surface insolation appears constant from an everyday's point of view but this quantity has been found to be changing in small scale that may lead to climate change over an extended period of time. However, the factors impacting this variance are always a subject of much debate. In long term observations for low air masses, the variation is governed by cloud cover, aerosol loading, relative humidity as well as water vapor content. Parallel observations in high air masses for the variation of received solar radiation are rather lacking. To fill up the existing gap, this paper aims to investigate the diurnal evolution of solar radiation spectrum in UV, PAR and NIR bands in high air masses. In the current work, a total of 25 days of global and diffuse solar spectrum ranges from air mass 2 to 6 were collected using shadowband technique. It is found that the evolution pattern for all spectral components follows a high coefficient of determination with respect to global radiation. The result analysis also shows that variation of solar radiation is the least in UV fraction, followed by PAR and the most in NIR fraction. It is deduced that the broader amplitude of fraction in PAR and NIR because they incorporate variation of aerosol and water vapor. Decreasing trend in NIR fraction for constant UV fraction is likely associated to the increase of water vapor content. While reduction of PAR fraction for specific air mass interval is due to the increase in aerosol loading.

INTRODUCTION

Solar surface insolation represents the amount of solar radiance reaches the Earth's surface in a specified area. It has important implications in various fields such as solar renewable energy (Escobedo et al. 2011), photovoltaic module (Gottschalg et al. 2003), wastewater treatment (Mehrdadi et al. 2007), climate change (Wang et al. 2011), wind flow structure and pollutant dispersion (Wang et al. 2011). Previous studies revealed that clouds are the major modulator of solar radiation reaching the land surface; evident by findings from satellite data that the surface solar radiation increased at a rate of 0.16W/m^2/yr since 1990, which is consistent with decreasing cloudiness observed from satellite (Pinker et al. 2005). Another opinion for the attenuation of solar radiance is related to greenhouse gases (GHGs). Ambiance change in relative humidity is also suspected to have an effect on its depletion. It is reported that decreasing water vapor may be responsible for decreasing global radiation in China. Under cloud-free condition, increased anthropogenic aerosol loading from emissions of pollutants is responsible for decreased surface solar radiation (Qian et al. 2006). However, disagreement is found by Wang et al. (2011) that negative surface solar radiation trends before 1990 in China can be attributed to increase in aerosol loading, but failed to explain the trend reverses after 1986 while there is no sufficient evidence that aerosols are decreasing in these regions in the recent years. This is further verified in the Tibetan Plateau where the aerosol load contributed by human activities is still negligible, but its decreasing rate in solar radiation was much larger in magnitude than the whole China (Tang et al. 2010).

Prominently, the variation of solar radiation perceived at Earth's surface could be attributed to various impacting factors. It is fairly accepted that surface solar radiation negatively correlates with the total cloud amounts and near surface water vapor especially in regions at higher altitudes. However, the relationship between surface solar radiation changes and aerosol or water vapor changes are still under much debate (Wang et al. 2011). Decrease in solar radiation still cannot be fully explained neither by the increase of aerosol loading nor decrease in water vapor.

In the past literature, long term variation of solar insolation in low air masses had been routinely investigated and widely studied (Kun Yang & Koike 2002, Yeom et al. 2012, Kun Yang et al. 2006, Streets et al. 2006) but parallel observations in high air masses are not frequently monitored. Besides that, producing frequent insolation with high accuracy retrievals is important in various fields, including cli-

Fig. 1: Experimental set-up over the study area Tun Mustapha Tower (116°E, 6°N, 7.844 m above sea level).

mate change induced temperature rise (Ashrafi et al. 2012), numerical weather prediction, real-time monitoring of surface vegetation and evapotranspiration studies (Yeom et al. 2012). Therefore, to fill out the observational gap for frequent insolation prediction, diurnal variation of solar radiation in UV, PAR and NIR bands in high air masses is investigated in this paper. Also highlighted in this paper are the effects of atmospheric aerosol and water vapor on solar radiation spectrum.

MATERIALS AND METHODS

Data and measurement site: In this study, the solar spectrums were collected at Tun Mustapha Tower, Kota Kinabalu (116°E, 6°N, 7.844m above sea level) from 1st April to 31st May 2012. This site was selected because it has a clear view of sunrise to ensure that the solar pathway is not blocked by irrelevant objects or artificial buildings. Fig. 1 shows the experimental set up over the study area where the global, and diffuse, solar radiation was measured by LR-1 spectrometer (ASEQ, Canada) using shadowband technique. Table 1 presents the range of detectable wavelength and other important specifications of the unit.

Measurements were taken every 3 minutes averages. The analysis interval for each day was selected by the air mass range from 2 to 6. This range of air mass is typically associated to the hours just after sunrise from 0640 to 0815 hours. For lower air masses, they are not used because the rate-of-change of air mass and solar irradiance is small, failed to exemplify the variation of solar irradiance in long defined range. Besides that, only morning values were used because the afternoon hours are often cloudy and overcast. On the other hand, higher air masses are avoided due to greater uncertainty in air mass caused by refraction corrections that are increasingly sensitive to atmospheric temperature profiles (Harrison & Michalsky 1994). In our processing, air mass, *m* is calculated based on geometrical solar zenith angle, which

Table 1: Specifications of ASEQ spectrometer.

Specifications	ASEQ LR-1 Spectrometer
Detector range	300-1100 nm
Resolution	< 3 nm (with 200 µm fiber) < 1 nm (with 50 µm slit)
Pixels	3648
Pixel size	8 µm × 200 µm
Pixel well depth	100,000 electrons
Signal-to-noise ratio	300:1
A/D resolution	14 bit
Fiber optic connector	SMA 905 to 0.22 numerical aperture single strand optical fiber
Exposure time	2.5 ms-10 s
CCD reading time	14 ms

is calculated based on Solar Position Calculator, provided by Institute of Applied Physics of the Academy of Science of Moldova (ARG 2012).

Data reduction and analysis techniques: Prior to investigating the diurnal evolution of solar spectrum, it is necessary to ensure that the variation should not conform to the effects of cloud loading or transits. Therefore, the raw data were reduced by performing a cloud-masking procedure. To avoid cloudy points from the entire data set, only spectrums with Du Mortier's nebulosity index (NI) and Perez's clearness index ε greater than 0.92 and 1.55, respectively were selected for further analysis as discussed in Chang et al. (2012). Both threshold values are pre-determined by Langley-plot analysis where corresponding indexes that give the highest correlation represent the most likely clear and stable atmosphere. Details of the data reduction procedure are not discussed here as it was meticulously explained in our previous work (Chang et al. 2012).

The combined algorithm identifies not only the sky type during the observation period but also serves as an objective algorithm that selects clear sky data points from a continuous time series. The fundamental algorithms for NI computation are shown as follows (Zain-Ahmed et al. 2002).

$$NI = \frac{1-{}^{I_{d,cl}}/_{I}}{1-CR} \quad ...(1)$$

The cloud ratio, is given as:

$$CR = \frac{I_{d,cl}}{\left[I_{d,cl}+\exp(-4\mathrm{mAr})\sin\alpha\right]}, \quad ...(2)$$

Where $I_{d,cl}$ represents the clear sky illuminance given by:

$$I_{d,cl} = 0.0065 + (0.255 - 0.138\sin\alpha)\sin\alpha, \quad ...(3)$$

whereas Ar is the Rayleigh scattering coefficient written as:

$$Ar = \{5.4729 + m[3.0312 + m\{-0.6329 + m(0.091 - 0.00512m)\}]\}^{-1} \quad ...(4)$$

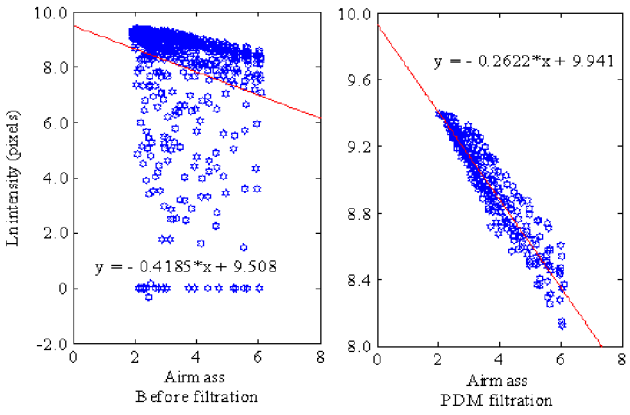

Fig. 2: Data reduction by cloud-masking algorithm.

and m is the optical air mass and α is the solar altitude. The Perez's model of clearness index, ε is calculated by (Djamila et al. 2011).

$$\varepsilon = \frac{\left(\left(I_{sd} + I_{dir}\right)/I_{sd}\right) + 1.041\emptyset_H}{1 + 1.041\emptyset_H}, \quad \ldots(5)$$

Where I_{dir} is the direct irradiance and $\emptyset_H$ is the solar zenith angle in radian.

The temporal evolution of the respective fractions to global is obtained directly using the measured spectrum in pixels. Each pixel measured by the unit in a given wavelength has an intensity value represented by a digital number. Though, it is not radiometrically calibrated, rationing both spectral segments yields a unitless parameter. Therefore, analysis of fraction of UV, PAR and NIR to global radiation can utilize the uncalibrated data in pixels.

Evolution of UV, PAR and NIR components of the solar spectrum is obtained by computing the fraction of each component to global solar radiation. It is determined by integrating the corresponding spectral segment in regards to the total measured:

$$F_n = \frac{\int_{\lambda_{n,1}}^{\lambda_{n,2}} I(\lambda)\, d\lambda}{\int_{\lambda_1}^{\lambda_2} I(\lambda)\, d\lambda}, \quad \ldots(6)$$

Where I and λ are the measured intensity and wavelength respectively. Subscript n denotes the corresponding spectral component (UV, PAR or NIR). In our division, fraction of UV, PAR and NIR are estimated in the range of 289.71 to 400nm, 400 to 700nm and 700-995.26 nm, respectively. The small spectral resolution (<0.1nm) allows accurate determination of definite integral using trapezoid rule of integration:

$$\int_{\lambda_1}^{\lambda_2} I(\lambda) = \frac{1}{2}[I(\lambda_1) + I(\lambda_2)][\lambda_2 - \lambda_1]. \quad \ldots(7)$$

RESULTS AND DISCUSSION

Raw data reduction by cloud-masking algorithm: In the data reduction process, the collected spectrums were assigned to an objective selection algorithm which consists of two models of sky classification; Perez-Du Mortier (PDM) model. The implementation of this selection algorithm is to ascertain only data exhibiting clear and cloudless skies are selected for the further analysis. Fig. 2 presents the progression of data reduction using PDM filtration. Initially, the raw data consist of n=730 data points, after the filtration by PDM it is reduced to n = 272 but better correlation, $r^2 = 0.88$ was remarked.

High correlation observed in the graph of solar intensity plot against air mass indicates that as air mass decreases in time evolution, solar radiation perceived at ground level increases proportionately. This is expected in normal solar evolution mechanism as the higher the air mass, more attenuations either by absorption or scattering due to Rayleigh contribution should be expected. In other words, the resulting pattern in Fig. 2 is justifiable to presume that the remaining data points favor a nearly clear sky or cloudless condition. These data points were then selected for further investigation on the diurnal evolution of solar spectrum in UV, PAR and NIR spectral components.

Evolution of UV, PAR and NIR spectral irradiance to global radiation: Fig. 3 shows the scatter plot between global solar radiation and spectral irradiances values of UV, PAR and NIR respectively. It is noted that in general positive relationship is found for all spectral components. Fitting obtained by linear regression of the observed points forcing the regression line intercept at origin indicates that highest correlation of $r^2 = 0.9952$ is observed in PAR segment, while UV remarks $r^2 = 0.8839$, and NIR $r^2 = 0.7831$. High coefficient of determination for all spectral components indicate that almost 100% of the total variance in UV, PAR and NIR can be explained in terms of increasing global radiation (Escobedo et al. 2011).

Detailed inspection of Fig. 3 suggests that higher scattering was observed in NIR and UV spectral component with respect to global radiation (G). For the NIR spectral component, one possible explanation could be due to the limited range of measureable wavelength. The unit measures only wavelength ranges from 300 to 1000nm, which does not cover the whole solar spectrum of NIR electromagnetic waves, hence resulting lower correlation coefficient. Nevertheless, its evolution pattern still significantly indicates that the variance of NIR irradiances is governed by the total global radiation.

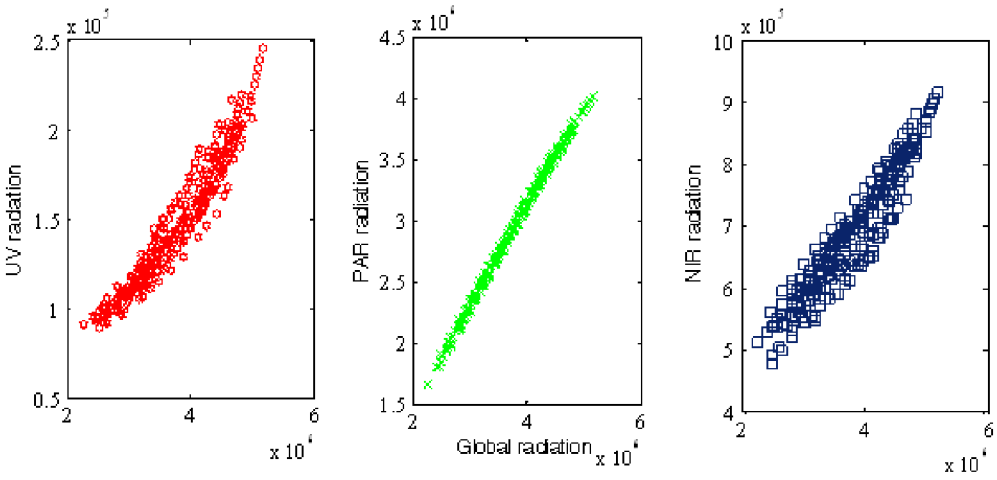

Fig. 3: Diurnal evolution of UV, PAR and NIR radiation to global radiation.

As for UV spectral component, instead of following a near-straight line regression, it increases exponentially with respect to G. Conversely, the variation of PAR spectral component follows a nearly perfect straight line evolution. This implies that the total variance in PAR has the highest portion associated to the evolution of global radiation in high air masses. This finding is in conjunction with results reported by Escobedo et al. (2011) such that highest correlation was remarked in PAR segment, followed by NIR and UV spectral.

Statistical analysis of fraction of UV, PAR and NIR to global: Fig. 4 shows the frequency distribution of UV, PAR and NIR fractions of G measured from air mass 2 to 6 over the study area after the filtration procedure. The fractions varied from 3.30 to 4.80% for UV/G, 72.10 to 81.20% for PAR/G and 14.40 to 22.80% for NIR/G. The frequency distribution follows a Gaussian distribution and the fraction corresponding to the maximum frequencies (3.60-3.90% for UV/G, 77.30-78.60% for PAR/G and 17.20-18.60% for NIR/G) match the mean fraction indicated in Table 2.

Broader amplitude of fraction occurs in PAR and NIR because they incorporate short time scale variation of aerosol and water vapor. Low variance in UV fraction is expected because daily averaged ozone concentration deviates only by very small amount, smaller deviation should be expected in diurnal evolution. Higher variance in NIR is associated to the possible change of relative humidity and temperature for decreasing air mass from 2 to 6; causing the concentration of water vapor changes notably. Aerosol mass loading is the dominant factor responsible for attenuation of solar radiation in PAR region. This indicates that variation of aerosol loading has considerable effects on solar radiation but its effects are relatively less momentous compared to total atmospheric water vapor columnar in high air masses.

Effects of atmospheric water vapor and aerosol on solar radiation spectrum: Measurements of atmospheric water vapor and aerosols in short time scale are implausible due to lack of frequent observation neither by satellite nor by ground base stations. Therefore, collected solar spectrum is separated into three segments (UV, PAR and NIR) and the corresponding temporal changes of their fraction to global is used to exemplify the variations of water vapor and aerosols in short time scale.

Fig. 5 presents the diurnal evolution of each segment to global radiation ranges from air mass 2 to 6. Evolution pattern over time for UV and PAR shared a similar pattern such that it increases with decreasing air mass. This is expected because the solar optical path length reduces for decreasing air mass, which in turn causes less attenuation of solar radiation either by absorption or scattering due to gaseous particles or air

Table 2: Statistical properties of G, UV, PAR and NIR observed between 1st April to 31st May 2011 over the study area.

Radiation component	Fraction to global (%)	Standard deviation	Mean (pixels)	Maximum (pixels)
UV	3.90E + 00	3.01E - 01	3.54E + 04	2.45E + 05
PAR	7.78E + 01	1.20E + 00	5.62E + 05	4.02E + 06
NIR	1.83E + 01	1.37E + 00	9.74E + 04	9.16E + 05
Global	-	-	3.79E + 06	5.18E + 06

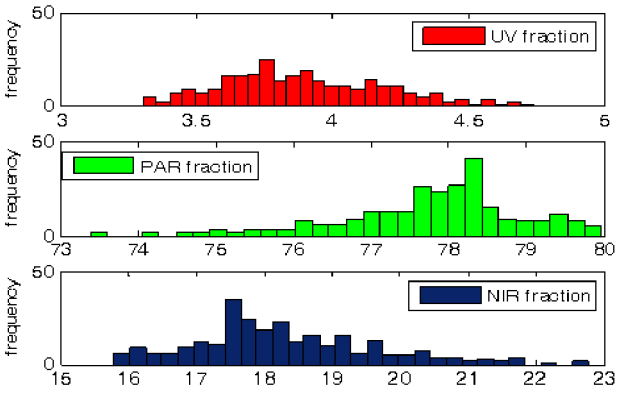

Fig. 4: Frequency distribution of UV, PAR and NIR fraction to global.

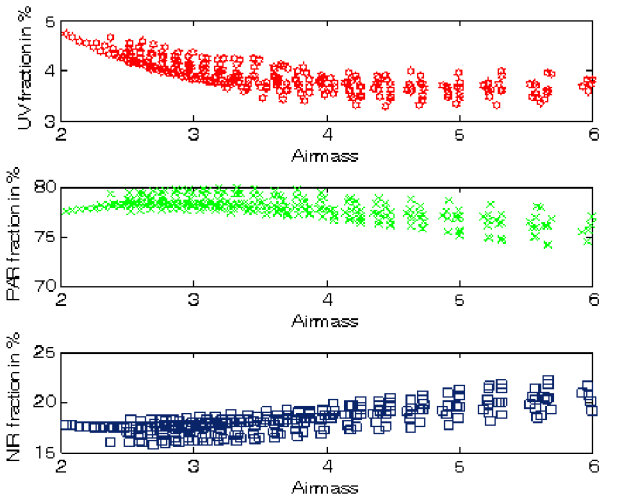

Fig. 5: Evolution of UV, PAR, and NIR fraction for air mass ranges from 2 to 6.

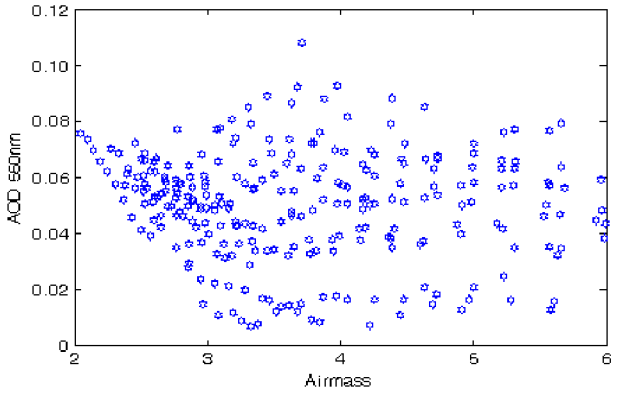

Fig. 6: Variation of AOD at 550nm wavelength from air mass 2 to 6.

molecules. This findings is in good agreement with results reported by Foyo-Moreno et al. (1998) where UV to broadband global radiation ratio increases with decreasing optical air mass.

However, a different pattern is observed in NIR fraction; it decreases when air mass reduces. One possible explanation for this pattern is likely corresponding to the increase of atmospheric water vapor present in air. NIR wavelengths are highly absorptive by water vapor and thus presence of great amount of which subsequently causes reduction of NIR in solar spectrum (Lombardi et al. 2011). Similar results were also reported by Wang et al. (2011) that due to the absorption of solar radiation by the atmospheric water vapor, increases in water vapor will cause decrease in surface solar radiation.

Given that water vapor absorbs more G than UV, therefore higher UV fraction could be associated to the presence of higher atmospheric water vapor content (Escobedo et al. 2011). Similar deduction could be applied to PAR and NIR fraction where water vapor absorbs more NIR than PAR hence simultaneous higher PAR and lower NIR fraction could be related to the presence of higher water vapor concentration. The statistical investigations of the present data support this premise that increasing trend of PAR fraction matches the decreasing trend of NIR fraction (Fig. 5). The decreasing trend in NIR fraction implies that as air mass decreases in time evolution, rate of extinction in NIR wavelengths increases in proportion due to increasing amount of water vapor.

Another interesting trend is observed that the negative slope in PAR fraction at air mass 3 (Fig. 5) does not correspond to steeper increase in NIR. Instead, it is associated to the increase of aerosol loading. The increasing trend of aerosol optical depth after air mass 3 matches the decreasing trend in PAR fraction (Fig. 6). Noted that the direct solar beam is also strongly affected by aerosol amount, presence of which in great amount significantly attenuates solar radiation either by absorption or scattering. Therefore, the steeper slope of decrease in PAR fraction at air mass 3 should be regarded of increasing amount of aerosols but not from the effects of water vapor.

Till this end, the prevailing justifications suggested that the variation of atmospheric water vapor in small scale time evolution is most significant in air mass ranges from 3 to 6, which is corresponding to times just after sunrise. This is within the expectation because sunrise heats up the atmosphere, causing rate of evaporation to increase accordingly and leading to higher amount of water content. Also, deducible is the variation of this parameter affects most in NIR wavelengths (16.48-20.69%), relatively lower in PAR (83.69-86.50%) and the least in UV (3.47-4.06%). This finding is also in good agreement with Xia et al. (2008) that in more humid conditions, absorption of solar radiation in the NIR region of the solar spectrum is enhanced, whereas

absorption in the UV region does not vary significantly. Detailed inspection of the result findings implied that under cloudless condition, diurnal evolution of solar radiation in high air masses could be subjected to both atmospheric water vapor and aerosol. This evolution, however, features a pattern that the depletion of solar insolation can be most likely associated to presence of water vapor and aerosol in ambient air.

CONCLUSION

In this study, diurnal evolution of solar radiation in UV, PAR and NIR wavelengths was investigated using solar spectrum ranging from air mass 2 to 6. It is found that the variance in all spectral components is mostly governed by the evolution of global radiation where PAR remarks the highest coefficient of determination. The statistical data analysis also suggests that UV fraction to global irradiance varies the least with 0.30, followed by PAR fraction, 1.20 and NIR fraction, 1.37. Higher variance is observed in PAR and NIR fraction because longer wavelengths of light are easily affected either by aerosol or water vapor content. Decreasing pattern observed in NIR fraction in time evolution is likely associated to increase of water vapor especially for day remarks with high temperature and low relative humidity, where the rate of evaporation is rapid. Although aerosol has lesser momentous effects on attenuation of solar radiation, its effects are still significant especially under cloud-free skies. The decrease in PAR fraction for constant NIR fraction is due to the effects of aerosols loading. Increase in aerosol loading causes more attenuations of solar radiation either by absorption or scattering especially in PAR regions, evident by the corresponding opposite trend between AOD and PAR fraction. As a preliminary justification, depletion of solar insolation is likely associated to presence of water vapor and aerosol in ambient air for high air masses.

REFERENCES

ARG, 2012. Sun calculator. Atmospheric Research Group, Institute of Applied Physics of the Academy of Science of Moldova. Available at: http://arg.phys.asm.md/index.html [Accessed September 10, 2012].

Ashrafi, K. et al. 2012. Prediction of Climate Change Induced Temperature Rise in Regional Scale Using Neural Network. Int. J. Environ Res., 6(3): 677-688.

Chang, J., Sentian, J. & Dayou, J. 2012. Perez-Du Mortier model of sky classification for Langley radiometric calibration at near sea-level sites. Submitted to Journal of Aerosol Science.

Djamila, H., Ming, C.C. & Kumaresan, S. 2011. Estimation of exterior vertical daylight for the humid tropic of Kota Kinabalu city in East Malaysia. Renewable Energy, 36(1): 9-15.

Escobedo, J.F. et al. 2011. Ratios of UV, PAR and NIR components to global solar radiation measured at Botucatu site in Brazil. Renewable Energy, 36(1): 169-178.

Foyo-Moreno, I., Vida, J. & Alados-Arboledas, L. 1998. Ground based ultraviolet (290-385 nm) and broadband solar radiation measurements in south-eastern Spain. International Journal of Climatology, 18(12): 1389-1400.

Gottschalg, R., Infield, D.G. & Kearney, M.J. 2003. Experimental study of variations of the solar spectrum of relevance to thin film solar cells. Solar Energy Materials & Solar Cells, 79(4): 527-537.

Harrison, L., Michalsky, J. 1994. Objective algorithms for the retrieval of optical depths from ground-based measurements. Applied optics, 33(22): 5126-32.

Lombardi, G. et al. 2011. A study of NIR atmospheric properties at Paranal Observatory. Astronomy & Astrophysics, 43: 1-7.

Mehrdadi, N. et al. 2007. Aplication of Solar Energy for Drying of Sludge from Pharmaceutical Industrial Waste Water and Probable Reuse. Int. J. Environ Res., 1(1): 42-48.

Pinker, R.T., Zhang, B., Dutton, E.G. 2005. Do satellites detect trends in surface solar radiation? Science, 308: 850-854.

Qian, Y. et al. 2006. More frequent cloud-free sky and less surface solar radiation in China from 1955 to 2000. Geophysical Research Letters, 33(L01812): 1-4.

Streets, D.G., Wu, Y., Chin, M. 2006. Two-decadal aerosol trends as a likely explanation of the global dimming/brightening transition. Geophysical Research Letters, 33, L15806(15): 1-4.

Tang, W.J. et al. 2010. Solar radiation trend across China in recent decades: a revisit with quality-controlled data. Atmospheric Chemistry and Physics Discussions, 10: 18389-18418.

Wang, C., Zhang, Z., Tian, W. 2011. Factors affecting the surface radiation trends over China between 1960 and 2000. Atmospheric Environment, 45(14): 2379-2385.

Wang, P. et al. 2011. Thermal Effect on Pollutant Dispersion in an Urban Street Canyon. Int. J. Environ Res., 5(3): 813-820.

Xia, X. et al. 2008. Annales Geophysicae Analysis of relationships between ultraviolet radiation (295-385 nm) and aerosols as well as shortwave radiation in North China Plain. Annales Geophysicae, 26: 2043-2052.

Yang, Kun & Koike, T. 2002. Estimating surface solar radiation from upper-air humidity. Solar Energy, 72(2): 177-186.

Yang, Kun, Koike, T., Ye, B. 2006. Improving estimation of hourly, daily, and monthly solar radiation by importing global data sets. Agricultural and Forest Meteorology, 137(1-2): 43-55.

Yeom, J.M., Han, K.S., Kim, J.J. 2012. Evaluation on penetration rate of cloud for incoming solar radiation using geostationary satellite data. Journal of Atmospheric Sciences, 48(2): 115-123.

Zain-Ahmed, A. et al. 2002. The availability of daylight from tropical skies -a case study of Malaysia. Renewable Energy, 25: 21-30.